Journal of Fluorescence, Vol. 9, No. 2, 1999

Effect of the External Refractive Index on Fluorescence Kinetics of Perylene in Human Erythrocyte Ghosts

Eugene P. Petrov,[1,2] Julia V. Kruchenok,[1] and Anatoly N. Rubinov[1]

Received August 31, 1998; accepted September 18, 1998

Fluorescence kinetics of perylene molecules in hemoglobin-free human erythrocyte membranes is investigated as a function of the refractive index of the external medium varied by adjusting the concentration of sorbitol or sucrose in an aqueous suspension of erythrocyte ghosts. It has been found that the fluorescence of perylene in erythrocyte ghosts decays nonexponentially, with the mean decay time decreasing from 7.13 to 5.70 ns with an increase in the refractive index of the suspension from 1.333 to 1.442. An analysis of the dependence made it possible to obtain an estimate of the second-rank orientational order parameter of perylene in the human erythrocyte membrane $\langle P_2 (\cos\theta)\rangle = 0.32 \ldots 0.43$, which bears witness of considerable ordering of perylene molecules along acyl chains of phospholipids constituting the membrane. Good correspondence of the order parameter with the value of the steady-state emission anisoptropy of perylene in erythrocyte ghosts suggests that acyl chains of phospholipids in the human erythrocyte membrane are predominantly oriented along the normal to its surface.

KEY WORDS: Excited-state lifetime; fluorescence decay time distribution; refractive index; human erythrocyte ghosts; perylene.

INTRODUCTION

Since the pioneering work of Purcell [1] it is understood that, according to Fermi's "golden rule," properties of the spontaneous emission depend not only on the quantum-mechanical parameters of the emitter, but also on the density of propagating photon modes in the emitter's optical environment. However, only in recent years has it been realized that mesoscopic dielectric structures can substantially change the photon density of states as compared to the free space (electromagnetic vacuum) and thus can modify spontaneous emission spectra and decay rates. The effect has far-reaching implications in science and technology, which induces the growing interest in the phenomenon (for review, see, e.g., Refs. 2 and 3). A number of theoretical investigations on modification of the spontaneous emission in optically inhomogeneous media have been published in recent years (see, e.g., Refs. 4–6 and refs. therein). To date, experiments in this field include, but are not limited to, studies of emission in the vicinity of a dielectric interface [7] and in dielectric slabs [8,9], Fabri–Perot microcavities [10,11], liquid microdroplets [12], water-in-oil micelles [13], and 3D dielectric lattices [14,15].

As regards biologically related structures, Toptygin *et al.* [16–18] were the first who realized that the classical theory developed by Lukosz [4] for spontaneous emission from thin dielectric layers can be successfully applied to fluorescent probes in lipid membranes. A simple quantum-mechanical description of the phenomenon whose predictions coincided with those of the classical model was proposed in Ref. 17. Recently, Cho [19] presented a quantum-electrodynamical description of the spontaneous emission from a thin lipid bilayer surrounded by water

[1] B. I. Stepanov Institute of Physics, National Academy of Sciences of Belarus, F. Skaryna Avenue 68, Minsk 220072, Belarus.
[2] To whom correspondence should be addressed.

1053-0509/99/0600-0111$16.00/0

with an explicit account for the frequency dependence of the (complex-valued) dielectric constants of water and lipid from the near-UV to the microwave region. Predictions of the quantum-electrodynamical model for the visible range are close to those of the classical and quantum-mechanical models. All three models predict a dependence of the radiative rate of a dipole in a dielectric layer on its orientation with respect to the normal to the interface.

In has been shown both theoretically and experimentally [16,17] that, due to orientation dependence of the radiative rate of a dipole in a dielectric layer, the spontaneous emission decay of a fluorescent probe in a lipid membrane is generally nonexponential, with the mean fluorescence lifetime depending on refractive indices of the membrane and surrounding medium and the angular distribution of probe molecules within the bilayer; the theory also predicts a nonmonotonic temperature dependence of the steady-state intensity of the probe fluorescence. Results of experimental investigations of 1,6-diphenyl-1,3,5-hexatriene (DPH) fluorescence in phospholipid bilayers were successfully applied in Refs. 16–18 to the evaluation of the second-rank orientational order parameter of DPH in the bilayer. Although there exist alternative explanations of the nonexponential fluorescence decay of DPH in biological membranes (see, e.g., Ref. 20), the theoretical predictions have a general character and should hold for any fluorescing molecule located within a bilayer. Indeed, Krishna and Periasamy [21] have recently observed a dependence of the fluorescence lifetime of another three fluorescent probes localized in a lipid bilayer on the refractive index of the surrounding medium. It should be noted that effects predicted by the theory were observed experimentally for fluorescent probes in lipid membranes back in the 1970s. Thus, in experiments with perylene in phospholipid bilayers, nonexponential fluorescence decays [22] and a temperature dependence of the fluorescence intensity [23] similar to that predicted and experimentally investigated for DPH in [16] have been observed.

In the present article, we report on an experimental observation of a dependence of fluorescence kinetics of perylene embedded in hemoglobin-free human erythrocyte ghost membranes on the refractive index of the surrounding medium.

OBJECTS OF INVESTIGATION

Perylene is a rigid aromatic molecule whose quantum yield in degassed solutions is close to unity [24]. The absorption dipole moment of perylene corresponding to the excitation within the first absorption band is parallel to the long symmetry axis of the molecule [25]. Upon passing to the excitation at shorter wavelengths, the absorption dipole makes a progressively larger angle with the axis. It has been found recently that, due to the nonplanar conformation assumed by perylene upon the $S_0 \rightarrow S_1$ electronic transition, the emission dipole makes an angle $\delta \approx 17°$ with the molecular plane in the ground state, thus resulting in the initial emission anisotropy $r_0 \approx 0.35$ [25, 26]. The nonpolar perylene molecule is widely used in investigations of the structure and dynamics of model and biological membranes [27].

In the present work, hemoglobin-free human erythrocyte membranes were used as an object of investigation. The erythrocyte cell can be presented as a disk with a diameter of ~8 μm and thickness of ~2 μm [28]. This shape is generally retained by the erythrocyte membrane (ghost) after hemolysis of the erythrocyte cell. Values in the range of 55–100 Å have been reported for the thickness of the erythrocyte membrane [29–31]. It should be noted that there is a difference between phospholipid bilayer membranes and the erythrocyte membrane: the latter contains, in addition to phospholipids, proteins constituting about 50% (w/w) of the erythrocyte membrane [32]. However, internal proteins entering into the composition of the erythrocyte membrane take only less than 20% of the area of the hydrophobic region of the membrane [31, 32], and therefore, one can effectively consider the fluorescent probe in the erythrocyte membrane as being mainly "dissolved" in the phospholipid bilayer.

The protocol used for producing erythrocyte ghosts (*vide infra*) provided predominant formation of ghosts having holes with a radius of the order of 50 Å [29], which ensured diffusion of substances dissolved in the suspension through the hole into the interior ghost volume, which provides an identical dielectric environment for both membrane surfaces.

Thus, taking into account that the thickness of the erythrocyte membrane is by about three orders of magnitude smaller than its lateral dimensions and small compared to the optical wavelength, the membrane can be considered to a good approximation as a plane loss-free dielectric layer. Therefore, the theory [4,17] can be applied to the spontaneous emission of the fluorescent probe localized inside the erythrocyte membrane.

FLUORESCENCE OF A PROBE IN A THIN DIELECTRIC LAYER

Generally, if a dipole capable of emitting light of wavelength λ is located within a thin ($nd << \lambda/8$) dielec-

tric layer with the refractive index n which is surrounded by a dielectric medium with the refractive index n_{ext}, the spontaneous emission rate of the dipole appears to be dependent on the angle θ it makes with the normal to the layer surface [4,17]:

$$k_{rad}(\theta) = k^0_{rad} f^2 n_{ext} \left(\sin^2\theta + \left(\frac{n_{ext}}{n}\right)^4 \cos^2\theta \right) \quad (1)$$

where k^0_{rad} is the spontaneous decay rate of the molecule *in vacuo*, n and n_{ext} are the refractive indices of the membrane and the surrounding medium, respectively, and f is a local-field correction factor depending on the refractive index and geometry of the local environment of the fluorescing center.

In the case of a fluorescent probe located within a phospholipid bilayer, one should take into account the angular distribution of probe molecules and their rotational diffusion. It has been shown in Ref. 16 that generally the rotational diffusion and the intensity decay cannot be uncoupled, and to obtain time dependences of the fluorescence intensity and emission anisotropy one needs to solve a rotational-diffusion-and-decay equation. In this case, nonexponential fluorescence decay of the probe is expected, which is described by the (continuous or discrete) distribution of decay constants. However, in particular cases of very slow and very fast (compared to the excited-state population decay) rotational diffusion, one can obtain approximate expressions which relate to the high accuracy of the mean fluorescence lifetime of a probe with its orientational distribution within the bilayer (specifically, the second-rank orientational order parameter $\langle P_2 \rangle$ [33, 34]) and the internal and external refractive indices. In the above cases, the inverse of the mean decay time of a rodlike probe whose absorption and emission dipole moments are parallel to the symmetry axis of the molecule is given by the formula

$$1/\bar{\tau} = k_{nr} + \gamma n_{ext} \left[1 - \langle P_2 \rangle + \left(\frac{n_{ext}}{n}\right)^4 \left(\langle P_2 \rangle + \frac{1}{2} \right) \right] \quad (2)$$

where k_{nr} is the rate of nonradiative depopulation of the excited state, $\gamma = 2k^0_{rad} f^2/3$, and $\langle P_2 \rangle = \langle (3\cos^2\theta - 1)/2 \rangle$ is the second-order Legendre polynomial averaged over the angular distribution of probe molecules in the membrane.

In our experiments, we used perylene, whose absorption dipole moment corresponding to the excitation wavelength employed in the present work ($\lambda_{ex} = 390$ nm) was oriented parallel to the long symmetry axis. However, as noted earlier, the emission dipole moment in this case is rotated by an angle $\delta \approx 17°$ with respect to the absorption dipole. Using an approach similar to that presented in Ref. 16, one can obtain an analogue of Eq. (2) for a fluorescent probe whose emission dipole moment makes an angle δ with the long symmetry axis:

$$1/\bar{\tau} = k_{nr} + \frac{1}{2}(1 - P_2(\cos\delta))\gamma n_{ext} \times \left[2 + \left(\frac{n_{ext}}{n}\right)^4 \right] + P_2(\cos\delta)\gamma n_{ext} \times \left[1 - \langle P_2 \rangle + \left(\frac{n_{ext}}{n}\right)^4 \left(\langle P_2 \rangle + \frac{1}{2} \right) \right] \quad (3)$$

It should be noted that Eqs. (2) and (3) can be applied only to a rodlike probe. In additon, in the case of Eq. (2) the probe is considered as rotating freely about its axis (for discussion, see Ref. 16). This is generally not applicable to perylene, which is known to behave as a strongly anisotropic rotor when dissolved in most solvents (see, e.g., Ref. 26 and references therein). However, experimental results of Jiang and Blanchard [35] suggest that in long-chain n-alcanes (n-C_9H_{20}, n-$C_{10}H_{22}$, n-$C_{12}H_{26}$, and n-$C_{16}H_{34}$), perylene behaves rather as a *prolate* rotor, i.e., long-chain aliphatic solvents constrain the perylene rotational motion to be predominantly about its longer axis. It should be noted that phospholipids constituting the human erythrocyte membrane have a C_{16}–C_{24} skeleton [36], i.e., their acyl chains are even longer than molecules of the above-mentioned n-alcanes. The nonpolar fluorescent probe perylene is known to localize within the hydrophobic region of the phospholipid bilayer [27], i.e., phospholipid acyl chains constitute the environment of perylene in a biological membrane. A similar conclusion on the preferential out-of-plane character of the rotational motion of perylene in phospholipid bilayers enriched with cholesterol was drawn by Cogan *et al.* [22], which also applies to the system under investigation, since the cholesterol-to-phospholipid molar ratio in the erythrocyte membrane is as high as ~1:1 [37]. Therefore, we have grounds to assume that Eq. (3) is applicable to the description of perylene fluorescence in hemoglobin-free human erythrocyte ghosts.

MATERIALS AND METHODS

Chemicals

Water was triple distilled. Sodium dihydrogen phosphate dihydrate ($NaH_2PO_4 \cdot 2H_2O$) (extra pure), *di*sodium hydrogen phosphate dodecahydrate ($HNa_2O_4P \cdot 12H_2O$) (analytic grade), Folin–Ciocalteu's phenol reagent,

sucrose (analytic grade), sorbitol (pharmacological grade), and tetrahydrofuran (Uvasol) were all purchased from Merck. Analytic-grade sodium chloride was purchased from Reakhim. Human serum albumin was research grade (98+%) from Serva. Perylene was purchased from Sigma and was used without further purification. Purified paraffin oil was a gift from Dr. N. A. Nemkovich.

Preparation of Erythrocyte Ghosts

All procedures were at 0–5°C (typically on ice), and all centrifugations were performed in a K24 cooled centrifuge (Heinz Janetzki, Germany). Blood [O(I) group] was obtained from normal adult donors. Hemoglobin-free human erythrocyte ghosts were prepared as described [37], except that the hemolysis buffer was 8 m*M* NaP_i, pH 7.4. Membranes were suspended for 10 min in this buffer before each centrifugation to allow hemoglobin to exit fully. Washed ghosts were resuspended in the 0.15 *M* NaCl solution and were stored at 5°C. The membrane suspension was used within 2 days. None of our results varied with the storage.

Labeling of Erythrocyte Membranes

Labeling of erythrocyte ghosts was carried out by injecting a 10^{-3} *M* solution of perylene in tetrahydrofuran into a vigorously stirred suspension of erythrocyte ghosts to yield a final concentration of 10^{-5} *M* perylene in the suspension. The suspension was incubated for 0.5 h at 25°C upon continuous vortexing, which provided conditions close to optimal for perylene binding to the phospholipid bilayer [38]. The excess of perylene was washed by centrifugation of the labeled suspension with 0.15 *M* NaCl at 13,000*g* for 15 min.

The final concentration of proteins in the diluted membrane suspension used in experiments was determined by the modified Lowry method [39] calibrated by a set of aqueous solutions of human serum albumin. The concentration of proteins in membrane suspensions was 0.5–1.5 mg/ml, which corresponds to $(1–3)\cdot10^9$ ghosts/ml. The concentration of perylene in samples estimated from absorption measurements was about $5\cdot10^{-7}$ *M*. The volume taken by membranes in the suspension can be estimated from the protein concentration measured, the average protein content per ghost [37], and the average volume of the erythrocyte membrane calculated from its surface area and thickness. The calculations yield a perylene concentration in membranes of $\sim(1–6)\cdot10^{-4}$ *M*.

Preparation of Membrane Suspensions in Media with Varying Refractive Indices

The external refractive index was varied by adjusting the concentration of sorbitol or sucrose in suspensions of erythrocyte ghosts. Membrane suspensions in media with desired carbohydrate concentrations were prepared according to the following protocol: a specified amount of sorbitol or sucrose was partially dissolved in 1 ml of an aqueous 0.15 *M* NaCl solution, then 560 μl of the concentrated ghost suspension was added, and the mixture was diluted with the 0.15 *M* NaCl solution to yield a volume of 3 ml.

The refraction of sorbitol solutions was measured on an RL3 Abbe-type refractometer with an accuracy of $\pm2\cdot10^{-4}$. Values of the refractive index of sucrose solutions were interpolated from data tabulated in Ref. 40.

Unlabeled membrane suspensions were tested for fluorescence. Since the impurity fluorescence coming from sucrose was found to be several times stronger than that from sorbitol impurities, most fluorescence experiments were carried out with sorbitol. The steady-state impurity fluorescence in suspensions containing sorbitol did not exceed 2% of the perylene fluorescence intensity.

Measurements of Erythrocyte Ghost Refractive Index

For refractive index measurements, a set of samples of the erythrocyte ghost suspension was prepared with varying concentrations of sucrose as described above. Sucrose solutions in the 0.15 *M* NaCl solution with corresponding concentrations were used as reference samples. Each of the samples used for refractive index measurements contained $\sim3\cdot10^9$ ghosts/ml. Eight sucrose concentrations were used to cover the refractive index range of 1.381 to 1.451.

Optical Measurements

The optical density of ghost suspensions was measured on a Specord M40 spectrophotometer (Karl-Zeiss Jena, Germany). Steady-state fluorescence emission and excitation spectra and fluorescence anisotropy were recorded on an SFL-1211A spectrofluorimeter (SOLAR, Minsk, Belarus).

Fluorescence kinetics were measured using the single-photon counting method on a PRA 3000 fluorometer (Photochemical Research Associates, London, Ontario) with the electric discharge in air used as an excitation source. The excitation wavelength was set to λ_{ex} = 390 nm. Fluorescence emission was collected at λ_{em} = 490

nm. Spectral slit widths of excitation and emission monochromators were set to 16 nm. Fluorescence decay traces and excitation lamp profiles were recorded in 511 channels with 0.16 ns/channel. The typical number of counts in a peak channel (CPC) in fluorescence kinetics was about $5 \cdot 10^3$.

Recovery of Fluorescence Decay Time Distributions

Fluorescence kinetics were analyzed by recovering underlying distributions of decay constants. This reduces to the solution of the following integral equation with respect to the distribution function of fluorescence decay constants $f(k)$, $k = 1/\tau$ being the fluorescence decay rate:

$$\int_{k_{\min}}^{k_{\max}} \left(\int_0^t R(t - t') \exp(-kt')dt' \right) f(k)dk = d(t) \quad (4)$$

Here $R(t)$ is the apparatus response function of the fluorometer, and $d(t)$ is the (noisy) fluorescence decay trace. The problem of the recovery of the distribution of decay constants is known to be ill posed, and a number of methods employing different kinds of regularization have been developed during the last decade (see, e.g., Refs. 41 and 42). In the present work, we used a regularized method recently proposed by Petrov [43]. A brief outline of the algorithm is presented in the Appendix. The convolution with the apparatus response was carried out using the local quadratic approximation of the apparatus response function [44]. The distribution function of decay rates recovered from the decay kinetics can easily be transformed to yield, e.g., a distribution function of preexponential factors on the scale of decay times.

In practice, a finite-dimensional approximation of Eq. (4) is solved, so that the fluorescence response $I(t)$ to an infinitely short excitation pulse is approximated by the exponential series

$$I(t) = \sum_{i=1}^{n} f_i \exp(-t/\tau_i) \quad (5)$$

In the method used in the analysis of fluorescence kinetics data, decay times are uniformly spaced on the logarithmic scale, which provides optimum resolution of the Laplace transform inversion [45]. In the analysis, $n = 100$ exponential terms with lifetimes spanning the range 0.08 ... 64.0 ns were used. Since no fluorescence buildup was expected for the system under investigation, distributions were computed subject to nonnegative constraints. Mean fluorescence decay times were calculated from decay time distributions by the following formula:

$$\bar{\tau} = \sum_{i=1}^{n} f_i \tau_i^2 \Big/ \sum_{i=1}^{n} f_i \tau_i \quad (6)$$

RESULTS AND DISCUSSION

We tried to estimate the average refractive index of erythrocyte ghosts by investigating the dependence of the optical density of the suspension on the value of the refractive index of the medium surrounding the membranes. The refractive index of the medium was changed by varying the sucrose concentration in the suspension while retaining the concentration of membranes at a constant value. Evidently, when the refractive index of the medium approaches that of the membranes, a minimum in the optical density should be observed due to a decrease in the efficiency of light scattering by the suspension. This procedure is applicable if the refractive index of membranes is unaffected by the substance dissolved in the suspension for adjusting the refractive index of the latter. As pointed out in the discussion below, this holds for erythrocyte membranes in sucrose and sorbitol solutions.

The optical density of the suspension of erythrocyte ghosts without perylene at 500 nm is presented in Fig. 1 as a function of the refractive index of the external medium adjusted by varying the sucrose concentration (sucrose solutions in water were used as reference samples). We have observed a steady decrease in the optical density of the suspension with increasing external refractive index n_{ext} from 1.381 to 1.451. In contrast to results reported in Ref. 17 for a lipid bilayer, we have found no minima

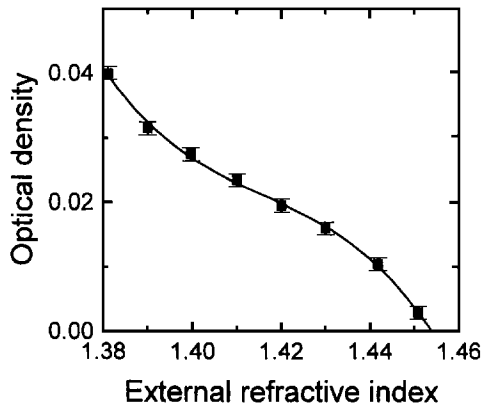

Fig. 1. (■) Optical density of erythrocyte ghosts suspension as a function of the refractive index of the aqueous sucrose solution. The curve is drawn as a guide for the eye. $\lambda = 500$ nm; temperature, 22 ± 2°C.

in the optical density within the above range of refractive index values. Therefore, we conclude that erythrocyte ghosts have a refractive index equal to or higher than that of the 64% aqueous sucrose solution, i.e., the lower estimate of the refractive index of the erythrocyte ghost membrane is 1.451. This value agrees with the dielectric constant of lipids $\epsilon = n^2 \sim 2.2$ [46] and the refractive index value of 1.454 reported for lecithin membranes [47] and the value of 1.504 measured for the erythrocyte membrane [48].

Steady-state fluorescence excitation (λ_{em} = 480 nm) and emission (λ_{ex} = 390 nm) spectra of perylene in erythrocyte ghosts are presented in Fig. 2. The value of the steady-state fluorescence anisotropy of perylene in erythrocyte ghosts measured at 20°C with the above excitation and emission wavelengths was $r_{ss} = 0.080 \pm 0.005$, which agrees well with anisotropy values report previously for fluorescence of perylene in human erythrocyte ghosts [52,53]. Evaluation of the fluorescence quantum yield was complicated by the presence of light scattering by membranes, which should be taken into account. However, the procedure outlined in Ref. 17 for evaluation of the quantum yield of a fluorescent probe in the presence of scattering cannot be applied to the system under investigation, since the size of an erythrocyte ghost lies in the range of about 2–8 μm, exceeding substantially the wavelength of light in the visible range, and the scattering indicatrix of erythrocyte ghosts is substantially stretched to the forward direction, as has been found in numerical calculations [49]. The value of 0.95 reported in Ref. 50 for perylene in phospholipid liposomes was used as an estimate of the perylene quantum yield in hemoglobin-free erythrocyte ghosts. This value of the quantum yield corresponds to a nonradiative decay rate of about $0.7 \cdot 10^{-2}$ ns^{-1}.

Fluorescence kinetics of perylene in erythrocyte ghosts was collected for the suspension without sucrose or sorbitol added and for six samples with different sorbitol concentrations and two samples with different sucrose concentrations. In all these cases, fluorescence decays exhibited slightly nonexponential behavior, with the mean decay time depending on the refractive index of the medium (Fig. 3). As a reference, we measured the fluorescence kinetics of perylene in paraffin oil (undegassed), which was found to decay exponentially with the lifetime of 4.67 ± 0.05 ns.

Fluorescence decays were analyzed by the decay time distribution technique described above and the results of such an analysis of perylene fluorescence from erythrocyte ghosts at three values of the external refractive index are presented in Fig. 4. For comparison, the narrow-peak distribution corresponding to the exponential decay of perylene in paraffin oil is shown as the gray area. The short-lived fluorescence, with a characteristic lifetime of ~1 ns, whose contribution to the steady-state emission did not exceed 2% at the highest sorbitol concentration was attributed to impurities in the buffer and sorbitol or sucrose. It should be noted that similar distributions of decay times were recovered by Prenner *et al.* [51] from fluorescence kinetics of DPH-labeled phospholipids incorporated into hemoglobin-free erythrocyte ghosts.

At the accuracy level of the fluorescence decay kinetics recorded in our experiments (CPC ~ $5 \cdot 10^3$), one evidently cannot hope to recover the structure and particular shape of the fluorescence decay time distributions for perylene in membranes. Moreover, we believe

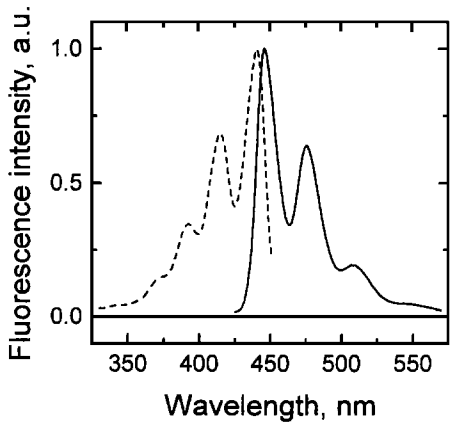

Fig. 2. Fluorescence emission (——) and excitation (---) spectra of perylene in hemoglobin-free erythrocyte ghosts. The excitation spectrum was recorded at λ_{em} = 480 nm; the fluorescence spectrum was excited at λ_{ex} = 390 nm. Temperature, 20 ± 2°C.

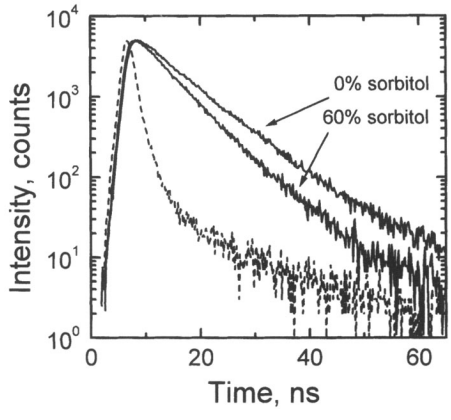

Fig. 3. Fluorescence decays of perylene in hemoglobin-free erythrocyte ghosts suspended in aqueous medium (n_{ext} = 1.333) and a 60% (w/w) aqueous solution of sorbitol (n_{ext} = 1.433). The dashed curve shows the apparatus response function of the fluorometer. λ_{ex} = 337.1 nm; λ_{em} = 480 nm. Temperature, 20 ± 2°C.

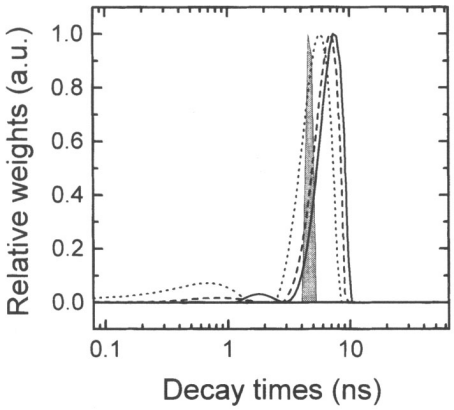

Fig. 4. Fluorescence decay time distributions recovered from intensity decays of perylene in hemoglobin-free erythrocyte ghosts suspended in aqueous medium (n_{ext} = 1.333) (——) and aqueous sorbitol solutions with concentrations of 23% (n_{ext} = 1.369) (---) and 60% (w/w) (n_{ext} = 1.433) (···). For comparison, the gray shape presents the decay time distribution corresponding to a single-exponential decay of perylene in paraffin oil. λ_{ex} = 337.1 nm; λ_{em} = 480 nm. Temperature, 20 ± 2°C.

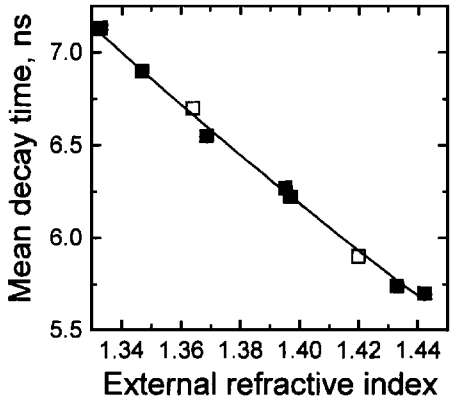

Fig. 5. Dependence of the mean fluorescence decay time of perylene in hemoglobin-free human erythrocyte ghosts suspended in aqueous sorbitol (■) and sucrose (□) solutions on the refractive index of the solution. λ_{ex} = 337.1 nm; λ_{em} = 480 nm. Temperature, 20 ± 2°C.

that even knowledge of the shape of decay time distributions would not help much in revealing the angular distribution of the probe, since the distribution of decay times can be theoretically predicted only in the case of "frozen" orientations of probe molecules, which does not hold for the case under investigation. The same reasoning, in our opinion, applies to the recovery of the probe's angular distribution function by the global analysis of a set of fluorescence decay traces recorded at different values of the external refractive indices. In this case, an analysis would reveal a hypothetical *static* distribution of probe orientations which provides the optimum fitting of the experimental data set. The result generally may have little (if anything) in common with the actual (dynamic) orientational distribution of fluorescent probe molecules.

Therefore, we have carried out an analysis of the dependence of the mean fluorescence lifetime on the external refractive index, for which much more definite theoretical conclusions can be drawn. The mean fluorescence lifetime of perylene in erythrocyte ghosts in the aqueous suspension without sorbitol or sucrose added was 7.12 ns, which is close to the value of 7.0 ns reported previously for the same system [54]. Values of the mean decay time recovered from experimental fluorescence kinetics are presented in Fig. 5 as a function of the refractive index of the solution. As is evident from Figs. 3–5, the mean decay time decreases with an increasing concentration of sorbitol or sucrose in the suspension of erythrocyte ghosts, i.e., with an increasing refractive index of the medium surrounding membranes.

It is evident from Fig. 5 that values of the mean decay time obtained for suspensions of perylene-labeled ghosts in sucrose solutions fall on the same curve as those in sorbitol solutions. Due to a substantial difference in molecular sizes, sorbitol and sucrose diffuse into the erythrocyte membrane at different rates and are accumulated there at different concentrations. However, the similar effect of both carbohydrates on the fluorescence lifetime of the probe suggests that the concentrations of carbohydrates accumulated in the erythrocyte membranes in our experiments are insufficient to induce substantial changes in its refractive index.

The dependence of the mean fluorescence decay time of perylene in erythrocyte ghosts on the refractive index of the external medium was analyzed by nonlinear fitting with Eqs. (2) and (3). In the analysis, two values of the refractive index of the erythrocyte membrane were used: the lower estimate, 1.451, obtained in the present work and the value of 1.504 from [48]. The analysis yielded the following values of the second-rank orientational order parameter $\langle P_2 \rangle$: 0.32 ± 0.03 (n_{ext} = 1.451) and 0.38 ± 0.03 (n_{ext} = 1.504) for the rod-like probe model Eq. (2) and 0.37 ± 0.03 (n_{ext} = 1.451) and 0.43 ± 0.03 (n_{ext} = 1.504) for the model accounting for an angle between the absorption dipole moment and the long symmetry axis of the perylene molecule Eq. (3).

In contrast to results obtained for the DPH fluorescence in phospholipid bilayers [17,18], the values of the parameter $\langle P_2 \rangle$ recovered in the present work for perylene in erythrocyte ghosts do not contradict the value of the steady-state anisotropy r_{ss} observed for this system. Indeed, the short- and long-time limiting anisotropy values r_0 and r_∞ for a fluorescent probe in a membrane are related by the formula [33,34]

$$r_\infty = r_0 \langle P_2 (\cos\theta)\rangle^2 \quad (7)$$

and estimates of the long-time limiting anisotropy based on the $\langle P_2 \rangle$ values recovered in the analysis lie within the limits of $r_\infty = 0.036 \ldots 0.064$, which agrees well with the steady-state anisotropy value $r_{ss} = 0.080 \pm 0.005$ observed in the present work. By assuming, for simplicity, isotropic rotation of the fluorescence probe in the membrane and applying the relationship for the hindered isotropic rotor [33,34],

$$r_\infty = r_{ss} - \frac{\phi}{\tau}(r_0 - r_{ss}) \quad (8)$$

one can obtain an estimate of the rotational correlation time of perylene in erythrocyte ghosts $\phi = 0.6 \ldots 1.3$ ns for model Eq. (2) and $0.3 \ldots 1.0$ ns for model Eq. (3), which has the same order as the values reported by Lakowicz and Knutson [55] for perylene in phospholipid bilayers at room temperature.

The agreement between the orientational order parameters estimated from the dependence of the perylene fluorescence lifetime on the external refractive index and fluorescence anisotropy of the probe in the membrane allows us to conclude that acyl chains of phospholipids constituting the human erythrocyte membrane are tilted insignificantly and are oriented predominantly along the normal to the membrane surface. This can be explained by the presence of the considerable amount of internal proteins and cholesterol in the human erythrocyte membrane. Indeed, it is well known that internal proteins of the membrane can influence the phospholipid packing considerably [36], whereas cholesterol is known to exert a substantial aligning effect on acyl chains of phospholipids (see, e.g., Ref. 56 and references therein).

Numerical simulations show that the decay time distributions presented in Fig. 4 are wider than the distributions which could result from an orientation-dependent fluorescence rate for the given refractive index ratio of 1.504 vs 1.333. To explain this, one either has to assume that the refractive index of erythrocyte membranes is of order 1.55 or higher or has to find another explanation for the phenomenon. As in Ref. 17, we are inclined to believe that this takes place mostly due to the distribution of local-field correction factors f [Eq. (1)], which should vary depending on the particular local dielectric environment of the probe (i.e., on its position and orientation with respect to the membrane surfaces or local inhomogeneities like internal protein molecules). Slightly nonexponential kinetics of perylene in phospholipid vesicles below the phase transition has also been observed by Holmes *et al.* [57], who assigned this to the perylene–perylene Förster energy transfer with a relatively low transfer efficiency. The parameters of the transfer, however, virtually did not change with increasing the concentration of the probe by two orders of magnitude. On the other hand, the Förster kinetics is described by a continuous lifetime distribution (see, e.g., Ref. 41), and at low transfer rates, it can fit virtually any slightly nonexponential kinetics with a narrow distribution of decay times. Thus, the problem of the lifetime heterogeneity of fluorescent probes in membranes still invites further investigation.

An interesting effect can be observed for a probe molecule for which the orientation of the absorption dipole moment with respect to the molecular symmetry axis depends on the excitation wavelength. For this probe, given an angular distribution of probe molecules in the ground state, the mutual effect of the anisotropic electromagnetic field of the exciting light in the membrane and the excitation wavelength dependence of the orientation of the absorption dipole moment will lead to a dependence of the angular distribution of excited molecules on the excitation wavelength and, thus, to the excitation wavelength dependence of the mean fluorescence lifetime. Perylene is just the probe of the type, and thus, in a lipid membrane it should exhibit such a dependence. Indeed, nonmonotonic variations of the fluorescence lifetime by a factor of ~1.5 with the excitation wavelength were observed in Ref. 58 for perylene in multilamellar phospholipid vesicles, which could be a manifestation of this effect. This conclusion is supported by the fact that the character of the dependence of the perylene lifetime on the excitation wavelength is not changed with pressure but changes substantially with the cholesterol concentration, which can be explained by the effect of cholesterol on the character of the rotational motion of perylene in the bilayer.

The orientational dependence of the radiative lifetime of a molecule in a thin dielectric layer should have an even more complex effect on fluorescence parameters of polar fluorescent probes. If the static dipole moment of such a probe increases upon electronic excitation, then upon pulsed optical excitation, the fluorescence spectrum of the probe undergoes a time-dependent Stokes shift due to the intermolecular orientational relaxation [59]. In this case, especially when the intermolecular relaxation takes place on a time scale close to the excited-state lifetime, one cannot uncouple the total fluorescence intensity decay and the time-dependent fluorescence shift due to the ν^3 dependence of the radiative rate [60]. As a result, the emission anisotropy of a polar probe in a membrane will be coupled to both the total intensity decay and the spectral relaxation of its fluorescence. In our opinion, this effect can lead to an emission wavelength dependence of

the time-resolved anisotropy of a polar probe in a membrane.

CONCLUSIONS

In the present work, we have carried out an investigation of fluorescence kinetics of perylene embedded in hemoglobin-free human erythrocyte membranes. Experiments with membrane suspensions in media with different refractive indices have shown that the fluorescence kinetics of perylene is nonexponential, with the mean fluorescence decay time decreasing from 7.13 to 5.70 ns with an increase in the refractive index of the medium surrounding the membrane from 1.333 to 1.442. The dependence of the fluorescence lifetime of the probe on the external refractive index is explained by a change in the density of modes of the electromagnetic field in the membrane compared to the free space. The second-rank orientational order parameter of perylene in the human erythrocyte membrane $\langle P_2(\cos\theta)\rangle$ estimated from the dependence of the fluorescence lifetime on the external refractive index lies within the range of 0.32 ... 0.43. The estimate of the orientational order parameter agrees well with the steady-state fluorescence anisotropy of perylene in the system under investigation, which suggests that acyl chains of phospholipids in the erythrocyte membrane are aligned predominantly along the normal to the membrane surface, which is explained by the effect of internal proteins and cholesterol in the human erythrocyte membrane. The nonexponential character of fluorescence decay kinetics of perylene in erythrocyte membranes is explained by the distribution of local field factors for probe molecules located at different binding sites.

APPENDIX[3]

In this section, we briefly outline the method [43] used for the analysis of fluorescence decays with minimum prior assumptions on the decay model. The recovery of a distribution of decay constants from fluorescence decay kinetics reduces to the solution of a finite-dimensional approximation of a Fredholm integral equation of the first kind (4), which leads to the solution of an overdetermined system of linear equations

$$\mathbf{Kf} = \mathbf{d} \tag{A1}$$

where $\mathbf{K}_{m\times n}$ is the finite-dimensional approximation of the kernel of integral Eq. (4), $\mathbf{d}_m$ is the (noisy) data vector, and $\mathbf{f}_n$ is the sought solution. Typical dimensions of the system of equations (A1) are $m = 500 \ldots 2000$ and $n = 50 \ldots 150$. Due to the Poisson character of the photon-counting noise, root-mean-square deviations of components of the data vector $\mathbf{d}_m$ of the mean are estimated as square roots $d_i^{1/2}$ of its components. Therefore, to obtain a weighted least-squares solution to system (A1), one needs to scale rows of the system by left multiplication of the system by an $m \times m$ diagonal matrix, $\mathbf{G}_m = \mathrm{diag}\{d_1^{-1/2}, \ldots, d_m^{-1/2}\}$ [62]. A more stable recovery of distributions of decay constants can be achieved if the columns in the matrix $\mathbf{A}$ are scaled by right multiplication of the matrix $\mathbf{K}$ by an $n \times n$ diagonal matrix $\mathbf{H}_n$ [62]. Numerical simulations have shown that the optimum choice is $\mathbf{H}_n = C\ \mathrm{diag}\{k_1^\gamma, \ldots, k_n^\gamma\}$, where C is a positive constant and $\{k_i\}_{i=1}^n$ are decay constants of the discretized Laplace transform kernel. It has been found that $\gamma = 1/8$ provides the optimum recovery of both discrete and continuous distributions of decay constants.

Thus, the recovery of a distribution of decay constants reduces to the solution of the system of equations

$$\mathbf{Ax} = \mathbf{b} \tag{A2}$$

where

$$\mathbf{A} = \mathbf{GKH}, \qquad \mathbf{b} = \mathbf{Gd} \tag{A3}$$

In the method being described, a Tikhonov-regularized minimum-norm solution [61] to Eq. (A1) is sought as

$$\mathbf{x}_\alpha = \arg \inf_{\mathbf{x}}(\|\mathbf{Ax} - \mathbf{b}\|^2 + \alpha\|\mathbf{x}\|^2) \tag{A4}$$

where $\alpha \geq 0$ is the so-called regularization parameter. With the regularization parameter known, the regularized solution of (A2) can be obtained by solving the following system of equations [62]:

$$\begin{bmatrix} \mathbf{A} \\ \sqrt{\alpha}\mathbf{I} \end{bmatrix} \mathbf{x} = \begin{bmatrix} \mathbf{b} \\ \mathbf{0} \end{bmatrix} \tag{A5}$$

where $\mathbf{I}_n$ is the $n \times n$ identity matrix. Thus, finding a regularized solution to Eq. (A2) is reduced to the proper choice of the regularization parameter.

The matrix $\mathbf{A}_{m\times n}$ is strongly ill conditioned, which results from scaling properties of the Laplace transform. This is best seen from the properties of its singular value decomposition (SVD) [62]:

$$\mathbf{A} = \mathbf{U}\begin{bmatrix} \mathbf{S} & \mathbf{0} \\ \mathbf{0} & \mathbf{0} \end{bmatrix}\mathbf{V}^{\mathrm{T}} \tag{A6}$$

where $\mathbf{S}_n = \mathrm{diag}\{s_1, \ldots, s_n\}$ is a diagonal matrix with

[3] Results in this section were presented, in part, at the Vth International Conference on Methods and Applications of Flourescence Spectroscopy, Berlin, Germany, 21–24 September 1997.

nonnegative entries called singular values which are ordered such that $s_1 \geq \ldots \geq s_n \geq 0$, and $\mathbf{U}_{m\times m}$ and $\mathbf{V}_{n\times n}$ are orthonormal projectors consisting of the so-called left and right singular vectors. It has been shown by Bertero *et al.* [63] that singular values of the Laplace transform operator follow the approximate relationship

$$s_i \sim \sqrt{\frac{\pi}{\cosh i\beta}}, \qquad \beta > 0 \tag{A7}$$

and thus, no "natural" threshold in the singular values which would separate the signal from the contribution of noise can be found in this case [64]. Computations show that the behavior of singular values of the matrix **A** is very similar to that described by Eq. (A4). It has been found that, due to the exponential decrease in the singular values, the s_i/s_1 ratio becomes less than the computational accuracy at $i = k < n$, which can be considered as a practical rank of the matrix **A**. Due to the transformation (A3), k is data dependent and, at typical accuracy levels, usually does not exceed 20. Therefore, we compute only a partial SVD of matrix **A** using the NIPALS algorithm [67]. This method makes it possible to compute the first k singular values satisfying the condition $s_i/s_1 \geq \varepsilon$ and the corresponding left and right singular vectors.

The generalized cross-validation (GCV) technique [65, 66] is known to be an efficient method for finding the value of the regularization parameter without prior knowledge of the noise level in the data as a minimizer of a generalized cross-validation functional: $\alpha = \arg\min_{\alpha} V(\alpha)$. The GCV method is best formulated in terms of the singular value decomposition of the matrix of the system [66]. Therefore, with the SVD computed, one can easily determine the amount of regularization required to obtain a regularized solution to the system of equations.

It should be noted that the NIPALS algorithm makes it possible to compute the "economy-size" SVD of the matrix: $\mathbf{A} = \mathbf{U}_{m\times n}\,\mathbf{S}_n\mathbf{V}_{n\times n}$. Therefore, we use the form of the GCV functional $V(\alpha)$ taking into account the incomplete character of the SVD computed by the NIPALS:

$$V(\alpha) = \left[\sum_{i=1}^{k}\left(\frac{\alpha z_i}{s_i^2 + \alpha}\right)^2 + \left(\sum_{i=1}^{m} b_i^2 - \sum_{i=1}^{k} z_i^2\right)\right] \Big/ \left(\sum_{i=1}^{k}\frac{\alpha}{s_i^2 + \alpha} + (n - k)\right)^2 \tag{A8}$$

where z_i and b_i are components of the vectors $\mathbf{z} = \mathbf{U}^T\mathbf{b}$ and **b**, respectively.

This method yields solution-dependent values of the regularization parameter α and provides stable recovery of both discrete and continuous distributions of decay constants without prior assumptions on their shapes within a wide range of kinetic data accuracy levels. Extensive numerical simulations substantiated the applicability of the procedure outlined to the analysis of fluorescence decay data over a wide range of data accuracy levels. The method is implemented in the FORTRAN-77 language, and typically about 10 s of CPU time is required for solving a problem with the dimensions $m \times n = 1024 \times 100$ on a personal computer with a 166-MHz Pentium processor.

ACKNOWLEDGMENTS

Fruitful discussions with Dr. I. I. Kalosha and Dr. A. N. Ponyavina are appreciated. We are grateful to Dr. L. G. Astaf'eva and Dr. G. P. Ledneva for making available results of scattering computations. The assistance of K. Shingel with the refractive index measurements is acknowledged. This work was supported by Foundation for Basic Research of the Republic of Belarus Grant M96-063.

REFERENCES

1. E. M. Purcell (1946) *Phys. Rev.* **69**, 681.
2. C. M. Soukoulis (Ed.) (1993) *Photonic Bandgaps and Localization*, Plenum Press, New York.
3. E. Burstein and C. Weisbuch (Eds.) (1995) *Confined Electrons and Photons: New Physics and Applications*, Plenum Press, New York.
4. W. Lukosz (1980) *Phys. Rev. B* **22**, 3030–3038.
5. H. Khosravi and R. Loudon (1991) *Proc. R. Soc. London Ser. A* **433**, 337–352; **436**, 373–389.
6. H. P. Urbach and G. L. J. A. Rikken (1998) *Phys. Rev. A* **57**, 3913–3930.
7. J. K. Trautman, J. J. Macklin, T. D. Harris, and L. E. Brus (1996) *Science* **272**, 255–258.
8. R. E. Kunz and W. Lukosz (1980) *Phys Rev. B* **21**, 4814–4828.
9. G. L. J. A. Rikken (1995) *Phys. Rev. A* **51**, 4906–4909.
10. A. N. Rubinov and V. I. Nikolaev (1970) *Izv. Akad. Nauk SSSR Ser. Fiz.* **34**, 1308–1311.
11. F. De Martini, G. Innocenti, G. R. Jakobowitz, and P. Mataloni (1987) *Phys. Rev. Lett.* **59**, 2955–2958.
12. M. D. Barnes, W. B. Whitten, S. Arnold, and J. M. Ramsey (1992) *J. Chem. Phys.* **97**, 7842–7845.
13. P. Lavallard, M. Rosenbauer, and T. Gacoin (1996) *Phys. Rev. A* **54**, 5450–5453.
14. J. Martorell and N. M. Lawandy (1990) *Phys. Rev. Lett.* **65**, 1877–1880.
15. E. P. Petrov, V. N. Bogomolov, I. I. Kalosha, and S. V. Gaponenko (1998) *Phys. Rev. Lett.* **81**, 77–80.
16. D. Toptygin, J. Svobodova, I. Konopasek, and L. Brand (1992) *J. Chem. Phys.* **96**, 7919–7930.
17. D. Toptygin and L. Brand (1993) *Biophys. Chem.* **48**, 205–220.
18. D. Toptygin and L. Brand (1995) *J. Fluoresc.* **5**, 39–50.
19. M. Cho (1997) *J. Chem. Phys.* **107**, 4499–4506.
20. E. Gratton and T. Parasassi (1995) *J. Fluoresc.* **5**, 51–57.
21. M. M. G. Krishna and N. Periasamy (1998) *J. Fluoresc.* **8**, 81–92.

22. U. Cogan, M. Shinitzky, G. Weber, and T. Nishida (1973) *Biochemistry* **12**, 521–528.
23. D. Papahadjopoulos, K. Jacobson, S. Nir, and T. Isac (1973) *Biochim. Biophys. Acta* **311**, 330–348.
24. I. B. Berlman (1965) *Handbook of Fluorescence Spectra of Aromatic Molecules*, Academic Press, New York and London.
25. M. van Gurp, T. van Heijnsbergen, G. van Ginkel, and Y. K. Levine (1989) *J. Chem. Phys.* **90**, 4103–4111.
26. J. Szubiakowski, A. Balter, W. Nowak, A. Kowalczyk, K. Wiśniewski, and M. Wierzbowska (1996) *Chem. Phys.* **208**, 283–296.
27. G. E. Dobretsov (1989) *Fluorescent Probes in the Study of Cells, Membranes, and Lipoproteins*, Nauka, Moscow [in Russian].
28. J. S. Beck (1978) *J. Theor. Biol.* **75**, 487–501.
29. M. R. Lieber and T. L. Steck (1982) *J. Biol. Chem.* **257**, 11651–11659, 11660–11666.
30. R. Peters (1973) *Biophys. Biochim. Acta* **318**, 469–473.
31. V. G. Ivkov and G. N. Berestovskii (1982) *Lipid Bilayer of Biological Membranes*, Nauka, Moscow [in Russian].
32. G. Guidotti (1972) *Annu. Rev. Biochem.* **41**, 731–752.
33. G. Lipari and A. Szabo (1980) *Biophys. J.* **30**, 489–506.
34. C. Zannoni (1981) *Mol. Phys.* **42**, 1303–1320.
35. Y. Jiang and G. L. Blanchard (1994) *J. Phys. Chem.* **98**, 6436–6440.
36. A. A. Boldyrev, S. V. Kotelevtsev, M. E. Lanio, K. Alvarez, and P. Perez (1990) *Introduction to Biomembranology*, Moscow University Publishers, Moscow [in Russian].
37. J. T. Dodge, C. Mitchell, and D. J. Hanahan (1963) *Arch. Biochem. Biophys.* **100**, 119–130.
38. Z. I. Lalchev and K. S. Birdi (1988) *C. R. Acad. Bulg. Sci.* **41**, 49–51.
39. M. A. K. Markwell, S. M. Haas, L. L. Bieber, and N. E. Tolbert (1978) *Anal. Biochem.* **87**, 206–210.
40. R. M. C. Dawson, D. C. Elliot, W. H. Elliott, and K. M. Jones (1986) *Data for Biochemical Research*, 3rd ed., Clarendon Press, Oxford.
41. A. Siemiarczuk, B. D. Wagner, and W. R. Ware (1990) *J. Phys. Chem.* **94**, 1661–1666.
42. D. M. Gakamsky, A. A. Goldin, E. P. Petrov, and A. N. Rubinov (1992) *Biophys. Chem.* **44**, 47–60; Erratum (1992) *Biophys. Chem.* **45**, 194–195.
43. E. P. Petrov (1997) in *Proceedings of the Vth Internstional Conference on Methods and Applications of Fluorescence Spectroscopy*, Köster, Berlin, Paper P142.
44. J. Večer, A. A. Kowalczyk, and R. E. Dale (1993) *Rev. Sci. Instrum.* **64**, 3403–3412.
45. N. Ostrowsky, D. Sornette, P. Parker, and E. R. Pike (1981) *Opt. Acta* **28**, 1059–1070.
46. J. Requena and D. A. Haydon (1975) *Proc. R. Soc. Lond. A* **347**, 161–177.
47. R. J. Cherry, K. Hsu, and D. Chapman (1972) *Biochim. Biophys. Acta* **288**, 12–21.
48. R. Peters (1971) *Biochim. Biophys. Acta* **233**, 465–468.
49. L. G. Astaf' eva and G. P. Ledneva (1998) Personal communication.
50. M. Shinitzky and Y. Barenholz (1974) *J. Biol. Chem.* **249**, 2652–2657.
51. E. Prenner, A. Hermetter, G. Landl, H. Stütz, H. F. Kauffmann, and A. J. Kungl (1993) *J. Phys. Chem.* **97**, 2788–2792.
52. M. Kehry, J. Yguerabide, and S. J. Singer (1976) *Science* **195**, 486–487.
53. B. Rudy and C. Gitler (1972) *Biochim. Biophys. Acta* **288**, 231–236.
54. M. B. Feintein, S. M. Fernandez, and R. I. Sha'afi (1975) *Biochim. Biophys. Acta* **413**, 354–370.
55. J. R. Lakowicz and J. R. Knutson (1980) *Biochemistry* **19**, 905–911.
56. C. Karolis, H. G. L. Coster, T. C. Chilcott, and K. D. Barrow (1998) *Biochim. Biophys. Acta* **1368**, 247–255.
57. A. S. Holmes, D. J. S. Birch, K. Suhling, R. E. Imhof, T. Salthammer, and H. Dreeskamp (1991) *Chem. Phys. Lett.* **186**, 189–194.
58. P. L.-G. Chong, B. W. van der Meer, and T. E. Thompson (1985) *Biochim. Biophys. Acta* **813**, 253–265.
59. D. M. Gakamsky, A. P. Demchenko, N. A. Nemkovich, A. N. Rubinov, V. I. Tomin, and N. V. Shcherbatska (1992) *Biophys. Chem.* **42**, 49–61.
60. E. P. Petrov and A. N. Rubinov (1994) *Lietuvos Fizikos Žurnalas* **34**, 47–51.
61. A. N. Tikhonov and V. Ya. Arsenin (1986) *Methods for Solving Ill-Posed Problems*, 3rd ed., Nauka, Moscow [in Russian].
62. C. L. Lawson and R. J. Hanson (1974) *Solving Least Squares Problems*, Prentice–Hall, Englewood Cliffs, NJ.
63. M. Bertero, P. Boccacci, and E. R. Pike (1982) *Proc. R. Soc. Lond. A* **383**, 15–29.
64. M. Bertero, C. De Mol, and E. R. Pike (1985) in W.-M. Boerner, H. Brand, L. A. Cram, D. T. Gjessing, A. K. Jordan, W. Keydel, G. Schweirz, and M. Vogel (Eds.), *Inverse Methods in Electromagnetic Imaging, Part I*, D. Reidel, Dordrecht, pp. 319–328.
65. G. Wahba (1977) *SIAM J. Numer. Anal.* **14**, 651–667.
66. G. H. Golub, M. Heath, and G. Wahba (1979) *Technometrics* **21**, 215–223.
67. P. Geladi and B. R. Kowalski (1986) *Anal. Chim. Acta* **185**, 1–17.